

# Focusing, refraction, and asymmetric transmission of elastic waves in solid metamaterials with aligned parallel gaps

Xiaoshi Su<sup>a)</sup> and Andrew N. Norris

Mechanical and Aerospace Engineering, Rutgers University, 98 Brett Road, Piscataway, New Jersey 08854, USA

(Received 19 October 2015; revised 19 February 2016; accepted 15 March 2016; published online 30 June 2016)

Gradient index (GRIN), refractive, and asymmetric transmission devices for elastic waves are designed using a solid with aligned parallel gaps. The gaps are assumed to be thin so that they can be considered as parallel cracks separating elastic plate waveguides. The plates do not interact with one another directly, only at their ends where they connect to the exterior solid. To formulate the transmission and reflection coefficients for SV- and P-waves, an analytical model is established using thin plate theory that couples the waveguide modes with the waves in the exterior body. The GRIN lens is designed by varying the thickness of the plates to achieve different flexural wave speeds. The refractive effect of SV-waves is achieved by designing the slope of the edge of the plate array, and keeping the ratio between plate length and flexural wavelength fixed. The asymmetric transmission of P-waves is achieved by sending an incident P-wave at a critical angle, at which total conversion to SV-wave occurs. An array of parallel gaps perpendicular to the propagation direction of the reflected waves stop the SV-wave but let P-waves travel through. Examples of focusing, steering, and asymmetric transmission devices are discussed.

© 2016 Acoustical Society of America. [http://dx.doi.org/10.1121/1.4950770]

[MRH] Pages: 3386–3394

### I. INTRODUCTION

In recent decades acoustic and elastic metamaterials that exhibit extraordinary wave bearing properties absent in natural materials have attracted much research interest, such as negative refractive devices, gradient index (GRIN) lens, 2 and non-reciprocal devices.<sup>3,4</sup> Negative index materials can be realized based on the localized resonant structures as proposed by Liu et al.5 An alternative approach uses phononic crystal (PC) which can be tailored to allow phase velocity and group velocity point in opposite directions. 1,6,7 To achieve non-reciprocity for acoustic waves, Liang and coworkers<sup>8,9</sup> used nonlinearity to break the symmetry of physical laws under time reversal. The energy transmission efficiency is usually restricted by the conversion efficiency between the acoustic metamaterial and nonlinear medium, and can be enhanced by increasing the conversion efficiency. 10 Another way to achieve non-reciprocity is by breaking the spatial symmetry using linear acoustic metamaterial, 11-13 or by acoustic metasurfaces. 14

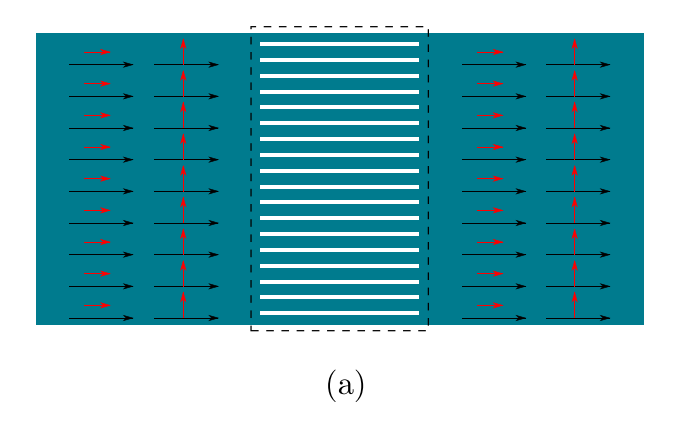
This paper focuses on the elastic analogue of GRIN lens, refractive, and asymmetric transmission devices. The physics behind elastodynamic waves is more complicated because of the coupling of different types of waves, but brings into play more interesting phenomena. Climente *et al.*<sup>15</sup> designed a GRIN lens for flexural waves based on the local variation of the plate thickness. Morvan *et al.*<sup>16</sup> experimentally demonstrated negative refraction of transverse waves with a two-dimensional (2D) PC of a square

In this paper, we model a solid with aligned parallel gaps as depicted in Fig. 1(a). The effect of the gaps is to make the solid material between them act like elastic plate waveguides. Unlike the PC or the locally resonant metamaterial, <sup>23,24</sup> our approach to the focusing, refraction and asymmetric transmission of elastic waves is based on the wave bearing properties of the plates. Broadband high transmission for refraction of elastic waves and multi-band high efficiency for asymmetric transmission are achieved. Similar to the idea of applying pre-compression differentially on granular chains to achieve phase delay, 25 we vary the thickness of the plates but keep the lengths constant to achieve a focusing effect. The wave bearing properties of the plates also lead to the idea of splitting P-wave and SV-wave in an elastic body by using an array of aligned parallel gaps. Our approach to asymmetric P-wave transmission uses the combination of the free boundary of a half-space and an array of aligned

3386

lattice with cylindrical cavities. Later, Pierre *et al.*<sup>17</sup> achieved negative refraction for antisymmetric Lamb waves with a similar design. The focusing of bending waves in perforated thin plates was realized by Farhat *et al.*<sup>18</sup> and Dubois *et al.*, <sup>19</sup> respectively. Zhu *et al.*<sup>20</sup> experimentally demonstrated the negative refraction of longitudinal waves by an elastic metamaterial with chiral microstructure fabricated in a steel plate. Chang *et al.*<sup>21</sup> used a soft hyperelastic material to split longitudinal and shear waves. Zhu *et al.*<sup>22</sup> proposed a 1D PC with anti-symmetric and symmetric unit cells that shows one-way Lamb wave transmission for both A and S modes. Most of these articles are concerned with flexural or Lamb waves, while only a few of them discuss bulk waves in elastic bodies, namely, P-, SV-, and SH-waves.

a)Electronic mail: xiaoshi.su@rutgers.edu



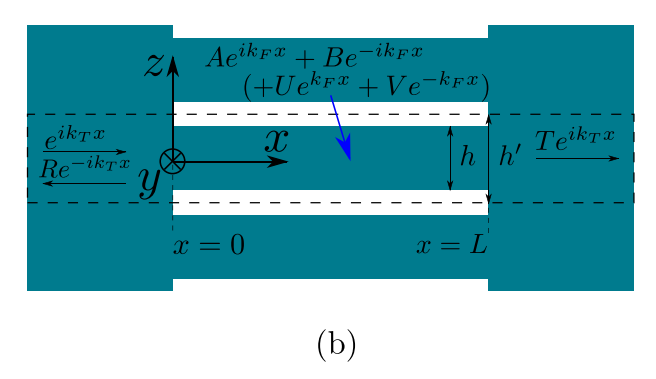


FIG. 1. (Color online) 2D schematic of aligned parallel gaps.

parallel gaps to achieve high and low energy transmission in opposite propagation directions. The models are simple and can be formulated analytically.

The outline of the paper is as follows. In Sec. II, we derive explicit expressions for transmission and reflection of normally incident SV- and P-waves, Eqs. (6), (7), (13), and (14). The properties of the plates and the design of GRIN lens are discussed in Sec. III. The refractive index for SV-and P-waves are derived in Sec. IV. Numerical examples showing zero-refraction of SV-waves and positive refraction of P-waves are also presented in Sec. IV. Mode conversion of P-waves in an elastic half-space at a free boundary and the condition for total conversion are discussed in Sec. V. The definition and numerical example of the asymmetric transmission effect using mode conversion is also given in Sec. V. Conclusions are presented in Sec. VI.

# II. TRANSMISSION THROUGH ALIGNED PLATES

# A. Governing equations

We consider the configuration of Fig. 1(a), in which an array of plates is connected to and separates two half-spaces. The configuration can be viewed as a homogenous solid with aligned thin gaps or cracks. At each of the junctions, the SV-wave in the half-space couples with the flexural wave on the plates, and the P-wave in the half-space couples with the compressional wave. In other words, an incident SV-wave (or P-wave) from the left side travels through the plate in the form of a flexural wave (or longitudinal wave), then transmits into the right side as SV-wave (or P-wave). To model and calculate the SV-wave (or P-wave) transmission and reflection coefficients, we only need to consider a single

plate element connected between two half-spaces, as shown in the boxed region in Fig. 1(b), because of the periodicity in the vertical direction. We model and formulate the problem using Kirchhoff plate theory which holds for long-wavelength flexural waves on thin plates. In this paper we focus on the frequency range in which the thin plate theory assumption is valid. Together with the boundary conditions: displacement (rotation angle) and force continuity at the two ends, we can establish six (or four) equations with six (or four) unknowns to solve for the transmission and reflection coefficients.

The density of the material is denoted by  $\rho$ , the Young's modulus by E, the shear modulus by  $\mu$ , and the Poisson's ratio by  $\nu$ . We also define the Cartesian coordinate system as shown in Fig. 1(b), where x is along the lateral direction of the plate, y is into the plane and perpendicular to x, and z is upward. The displacements in each direction are denoted as u, v, and w, respectively. The thickness of the plate is denoted by h, the width of the gap by a ( $a \ll h$ ), and the thickness of the unit structure in the boxed region in Fig. 1(b) is h' = h + a. The bending stiffness of the plate is  $D = Eh^3/12(1-\nu^2)$ . We assume the incident plane wave is independent of y-direction, i.e., there is no y-dependent term. The governing equations for flexural and longitudinal waves in the thin plate are

$$D\frac{\partial^4 w}{\partial x^4} - \rho h \omega^2 w = 0, \tag{1}$$

$$\frac{E}{1 - \nu^2} \frac{\partial^2 u}{\partial x^2} + \rho \omega^2 u = 0, \tag{2}$$

where  $\omega$  is the radial frequency, with time harmonic dependence  $e^{-i\omega t}$  assumed. The phase speeds of flexural and longitudinal waves  $(c_F, c_L)$  on the plate, and the phase speeds of SV- and P-waves  $(c_T, c_P)$  in the exterior body are

$$c_F = \left(\frac{Eh^2\omega^2}{12\rho(1-\nu^2)}\right)^{1/4}, \quad c_L = \sqrt{\frac{E}{\rho(1-\nu^2)}},$$

$$c_T = \sqrt{\frac{E}{2\rho(1+\nu)}}, \quad c_P = \sqrt{\frac{E(1-\nu)}{\rho(1+\nu)(1-2\nu)}}.$$
 (3)

# B. Transmission and reflection of a normally incident SV-wave

To solve for the transmission and reflection of SV-waves, we assume the amplitude of the displacement of the incident SV-wave as 1, reflected wave as R, transmitted wave as T, and on the plate as A, B, U, and V, see Fig. 1(b), so that

$$w = \begin{cases} e^{ik_T x} + Re^{-ik_T x}, & x < 0, \\ Ae^{ik_F x} + Be^{-ik_F x} & \\ +Ue^{k_F x} + Ve^{-k_F x}, & 0 < x < L, \\ Te^{ik_T (x - L)}, & x > L, \end{cases}$$
(4)

where  $k_F = \omega/c_F$  and  $k_T = \omega/c_T$  are the flexural and shear wavenumbers. Although  $\sigma_{xx}$  and  $\sigma_{yy}$  exist in the plate, they

do not contribute to the force on the plate since  $\int_{-h/2}^{h/2} \sigma_{xx} dz = -\int_{-h/2}^{h/2} [Ez/(1-\nu^2)] (\partial^2 w/\partial x^2) dz = 0$  and  $\int_{-h/2}^{h/2} \sigma_{yy} dz = -\int_{-h/2}^{h/2} [Ez\nu/(1-\nu^2)] (\partial^2 w/\partial x^2) dz = 0$ . Since there is no y-dependence in the governing equation the shear force per unit length in y-direction is  $Q = \int_{-h/2}^{h/2} \sigma_{xz} dz = -D(\partial^3 w/\partial x^3)$ . The shear force in the exterior body is  $Q = h'\sigma_{xz} = \mu h'(\partial w/\partial x)$ . The six z-averaged boundary conditions are continuity of displacement, rotation angle and shear force at x = 0 and x = L, which imply the following system of equations:

$$1 + R = A + B + U + V,$$

$$1 - R = \frac{k_F}{k_T} (A - B - iU + iV),$$

$$1 - R = \frac{hk_T}{h'k_F} (A - B + iU - iV),$$

$$T = Az^i + Bz^{-i} + Uz + Vz^{-1},$$

$$T = \frac{k_F}{k_T} (Az^i - Bz^{-i} - iUz + iVz^{-1}),$$

$$T = \frac{hk_T}{h'k_F} (Az^i - Bz^{-i} + iUz - iVz^{-1})$$
(5)

with  $z = e^{k_F L}$  so that  $z^{\pm i} = e^{\pm i k_F L}$ .

This system gives the transmission and reflection coefficients but the explicit expressions are long. We can split the solutions into symmetric and anti-symmetric modes which reduces the system to two  $3\times3$  systems. This leads to

$$T = \frac{1}{2}(R_S - R_A)e^{-ik_T L},\tag{6}$$

$$R = \frac{1}{2}(R_S + R_A)e^{-ik_T L},\tag{7}$$

where the reflection coefficients  $R_S$  and  $R_A$  are

$$R_{S} = \frac{\left(\frac{\tau}{\alpha} - \frac{1}{\tau}\right)\frac{1}{t_{h}} + \left(\frac{\tau}{\alpha} + \frac{1}{\tau}\right)\frac{1}{t} + i2}{\left(\frac{\tau}{\alpha} - \frac{1}{\tau}\right)\frac{1}{t_{h}} + \left(\frac{\tau}{\alpha} + \frac{1}{\tau}\right)\frac{1}{t} - i2},\tag{8}$$

$$R_{A} = \frac{\left(\frac{\tau}{\alpha} - \frac{1}{\tau}\right)t_{h} - \left(\frac{\tau}{\alpha} + \frac{1}{\tau}\right)t + i2}{\left(\frac{\tau}{\alpha} - \frac{1}{\tau}\right)t_{h} - \left(\frac{\tau}{\alpha} + \frac{1}{\tau}\right)t - i2},\tag{9}$$

with  $\tau = k_F/k_T$ ,  $\alpha = h/h'$ ,  $t = \tan(k_F L/2)$ , and  $t_h = \tanh(k_F L/2)$ . Note that  $R_S$  and  $R_A$  are both of unit magnitude, which implies that the transmission and reflection coefficients satisfy  $|T|^2 + |R|^2 = 1$ . Total transmission therefore occurs when  $R_S + R_A = 0$ . For small gap width, i.e.,  $\alpha \approx 1$ , |T| = 1 is obtained if  $k_F = k_T$  or if either of the following holds:

$$\tan(k_F L/2) \pm \tanh(k_F L/2) = 0. \tag{10}$$

However,  $k_F = k_T$  gives a single high frequency at which Kirchhoff plate theory does not hold. This single frequency is not in the frequency range of interest since we only consider long-wavelength flexural waves, i.e.,  $\lambda \gg h$ . The

frequencies satisfying Eq. (10) correspond to the symmetric (+) and anti-symmetric (-) modal frequencies for a plate of length L fixed at both ends, i.e., subject to the boundary conditions w = 0 and  $\partial w / \partial x = 0$ .

In this example, we consider an infinite aluminum domain (E=70 GPA,  $\nu=0.35$ , and  $\rho=2700\,\mathrm{kg/m^3}$ ) with an infinite array of aligned equidistant parallel gaps as shown in Fig. 1(a). The thickness and length of each plate are  $h=0.02\,\mathrm{m}$  and  $L=0.2\,\mathrm{m}$ , respectively. The geometric parameter  $h'=0.021\,\mathrm{m}$  is shown in Fig. 1(b). Figure 2 shows that flexural waves are quite dispersive on plates, it is also clear that the transmission tends to unity at high frequency.

# C. Transmission and reflection of a normally incident P-wave

Similarly, we can calculate the transmission and reflection coefficients of P-waves. Assuming the amplitude of the displacement of the incident wave as 1, reflected wave as R, transmitted wave as T, and the amplitude of displacement on the plate as A and B, the displacements are expressed as

$$u = \begin{cases} e^{ik_{P}x} + Re^{-ik_{P}x}, & x < 0, \\ Ae^{ik_{L}x} + Be^{-ik_{L}x}, & 0 < x < L, \\ Te^{ik_{P}(x-L)}, & x > L, \end{cases}$$
(11)

where  $k_P = \omega/c_P$  and  $k_L = \omega/c_L$  are the wavenumbers of P-wave in the exterior body and longitudinal wave in the plate. The compressional force in the exterior body is  $F_x = h'\sigma_{xx} = Eh'(\partial u/\partial x)$ , and the compressional force in the plate is  $F_x = Eh(\partial u/\partial x)$ . The four z-averaged boundary conditions are continuity of displacement and compressional force at x = 0 and x = L, yielding the system of equations,

$$1 + R = A + B,$$

$$1 - R = \frac{h}{h'} \frac{k_L}{k_P} (A - B),$$

$$T = Ae^{ik_L L} + Be^{-ik_L L},$$

$$T = \frac{h}{h'} \frac{k_L}{k_P} (Ae^{ik_L L} - Be^{-ik_L L})$$
(12)

The transmission and reflection coefficients for the incident P-wave are then

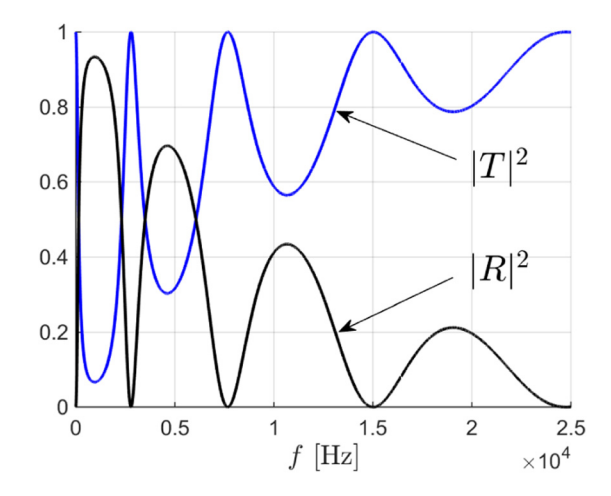


FIG. 2. (Color online) Transmission and reflection spectrum for a normally incident SV-wave.

$$T = \frac{4\alpha k_P k_L e^{ik_L L}}{(k_P + \alpha k_L)^2 - (k_P - \alpha k_L)^2 e^{i2k_L L}},$$
(13)

$$R = \frac{\left(k_P^2 - \alpha^2 k_L^2\right) \left(1 - e^{2ik_L L}\right)}{\left(k_P + \alpha k_L\right)^2 - \left(k_P - \alpha k_L\right)^2 e^{i2k_L L}},\tag{14}$$

which also satisfy  $|T|^2 + |R|^2 = 1$ . It is easy to show that total transmission, i.e., |T| = 1, requires either  $k_P - \alpha k_L = 0$  or  $e^{i2k_L L} = 1$ . The first occurs over all frequency range when  $\alpha = k_P/k_L = \sqrt{1-2\nu}/(1-\nu)$  and the others at  $\omega_n$ ,  $n = 1, 2, \ldots$ , where

$$\omega_n = \frac{n\pi}{L} \sqrt{\frac{E}{\rho(1-\nu^2)}}, \quad n = 1, 2, 3, ...,$$
 (15)

where  $\omega_n$  is the radial frequency corresponding to each n. However,  $\alpha = k_P/k_L$  indicates that total transmission can be achieved by choosing  $\nu$ , this only works for low Poisson's ratio material since we only interested in structures with small gap width.

We use the same structure and material as the example of SV-wave transmission. From Fig. 3, we find that the transmission is close to 1 over all frequencies so that P-waves transmit through these effective plates with high efficiency.

### D. Comparison of analytical results with simulation

The transmission spectrum for SV- and P-waves obtained using our analytical model and full wave FEM simulations are shown in Fig. 4 for comparison. For a normally incident SV-wave, the low frequency behavior of the analytical solution match well with simulation result, this indicates that our boundary condition assumptions are correct. The transmission peaks (|T|=1) shift at higher frequencies, this can be understood as the neck effect at the junction between plate and half space changes the effective length of the plates. However, the analytical model for P-waves is in good agreement with full FEM simulations, it is obvious that the transmission peaks match well in frequency.

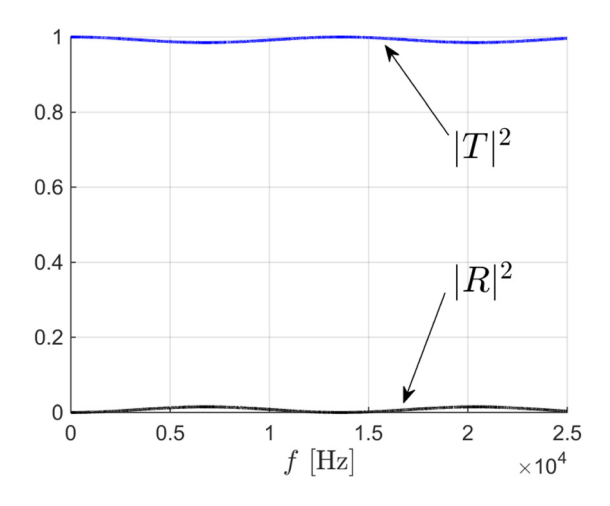
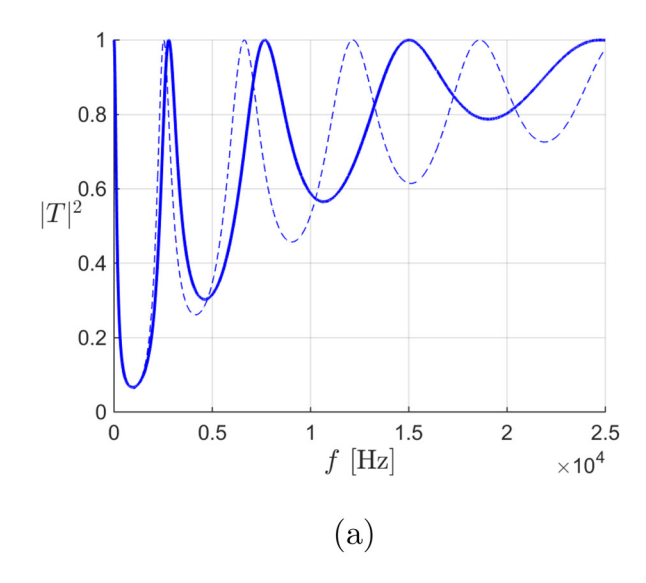


FIG. 3. (Color online) Transmission and reflection spectrum for a normally incident P-wave.



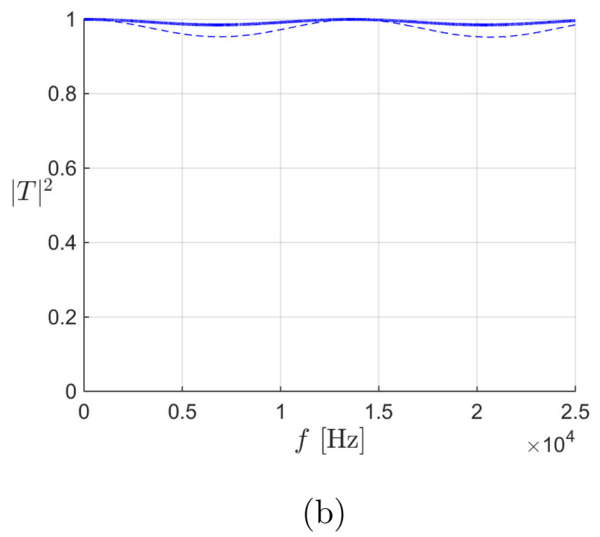


FIG. 4. (Color online) Comparison of the analytical solution (solid line) and full FEM simulation results (dashed line) for incident (a) SV-wave and (b) P-wave.

#### E. Improved analytical solution for SV-wave incidence

Since the analytically calculated P-wave transmission coefficient matches well with simulation results and is always high as long as the gap width a is small, i.e.,  $h/h' \approx 1$ , we only consider an improved analytical solution for SV-wave incidence. We introduce an empirical endeffect term  $\beta$  to represent the effective length of the plate  $L' = (1 + \beta)L$  and replace the L in our original model. The same geometry and the same material properties as the previous example are used to demonstrate how the modification works. The full wave FEM simulation is done using plate with h = 0.02 m and L = 0.2 m. Practically, L' is the length of the plate in the analytical model when we design a metamaterial, but L is the length which will be used in FEM simulation. By iterating the value of  $\beta$ , the analytical solution can be matched better to the full FEM solution at higher frequency range. Figure 5 shows good agreement by taking  $\beta = 0.07$ . This value of  $\beta$  only works for the parameters used in this example, new FEM simulations are required to find  $\beta$  for other parameter sets. However, the analytical

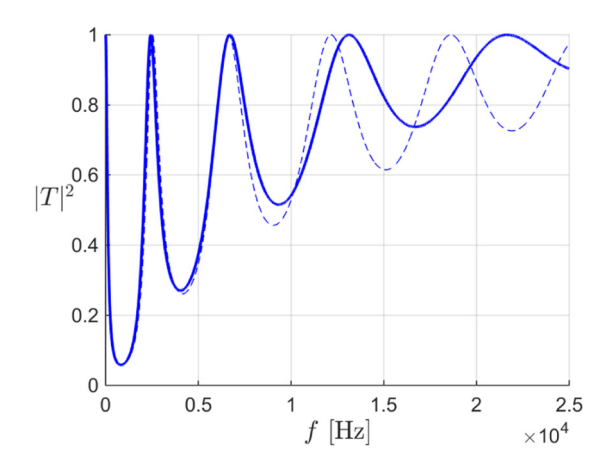


FIG. 5. (Color online) Comparison of the improved analytical solution (solid line) and simulation results (dashed line).

technique is still important since it helps understand the physics behind the model and provides an initial parameter set in our design. Alternatively, we can seek modification in simulations by changing the length of plates using  $L = L'/(1+\beta)$ .

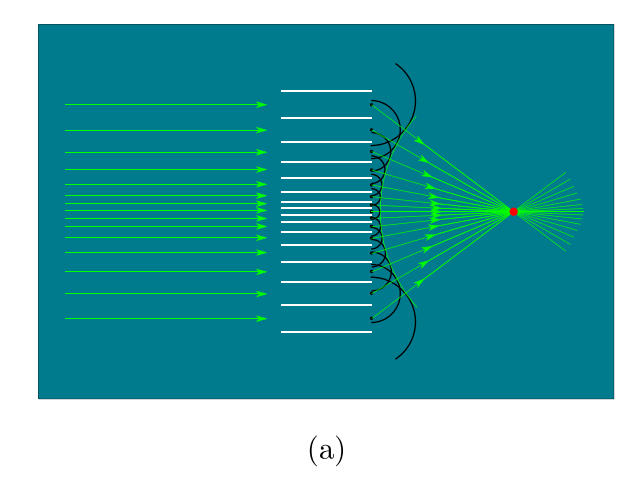
### **III. GRIN LENS FOR SV-WAVE**

#### A. Wave speeds and diffraction

We next design a GRIN lens, as depicted in Fig. 6(a), to focus SV-waves. The white strips are thin gaps, both of the ends are aligned vertically so that the effective plates have the same length. However, the thicknesses of the plates are allowed to vary based on the fact that flexural waves travel faster in thicker plates so that diffraction occurs earlier in thicker plates. Assuming circular wavefront radiating from the right end of each plate, the transmitted SV-wave intersect at the focal point according to Huygens' principle. The physics behind the focusing effect is based on diffraction effect similar to that in the generation of sound bullets.<sup>25</sup> The GRIN lens is designed by first selecting the thickness  $h_1$  and length L for the center plate, and choosing the distance d from the focal point to the end of the center plate at a particular frequency f. The gap width a is fixed. The total time for a flexural wave traveling from one end of a plate to the other end is  $t_F = L/c_F$ . As shown in Fig. 6(b), rays of the incident SV-wave from the left side travel along different paths but arrive at the focal point simultaneously. We formulate the relations between the thickness of the center plate and other plates as

$$\frac{\sqrt{h_{\text{total}}^2 + d^2} - d}{c_T} = \frac{L}{c_{F_1}} - \frac{L}{c_{F_i}},\tag{16}$$

where  $c_{F_1}$  is the flexural wave speed in the center plate and depends on  $h_1$ ,  $c_{F_i}$  is the flexural speed in the *i*th plate and depends on the thickness  $h_i$ ,  $h_{\text{total}}$  is the distance from the neutral line of the center plate to the neutral line of the *i*th plate which is accumulated by adding the thickness of each plate and width of gaps. Note that this type of lens is designed at a certain frequency for a chosen focal point, the focal distance will change if the frequency is changed.



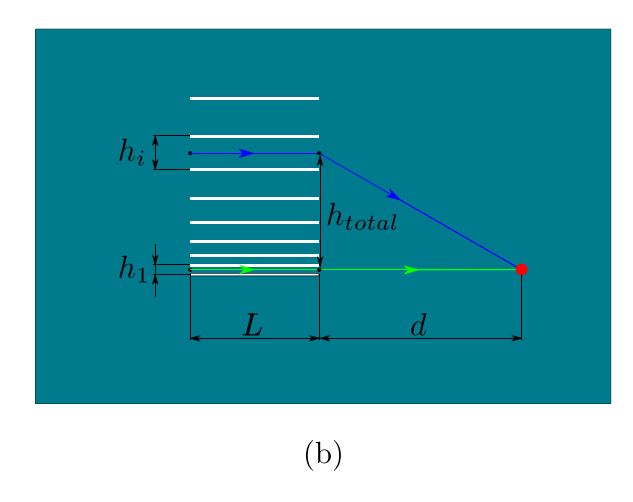


FIG. 6. (Color online) GRIN lens of a solid with parallel gaps.

## B. Example of GRIN lens for SV-waves

Aluminum ( $E = 70 \text{ GPA}, \nu = 0.35, \text{ and } \rho = 2700 \text{ kg/m}^3$ ) is used as the background material in our example. The width of each gap is a = 0.001 m, the length of each effective plate between gaps is chosen as  $L_1 = 0.2 \,\mathrm{m}$ , the thickness of the center plate is  $h_1 = 0.01$  m. The focal point is designed to be  $d = 0.2 \,\mathrm{m}$  away from the end of the center plate at  $40 \,\mathrm{kHz}$ . The thicknesses of other plates are calculated using Eq. (16). Since the plate thicknesses are varying, the end-effect correction for the effective plate lengths are also different. We take the same value of the modification term  $\beta$  for every plate for convenience, and iterate its value to achieve optimal focusing effect. The focal point in Fig. 7(c) is roughly 0.25 m away from the edge of plate array. Figure 7 shows that the focal point moves away from the plate array when the frequency increases, this is due to the phase speed of the flexural wave changing with frequency so that the phase gradient of the transmitted SV-waves also changes.

#### IV. REFRACTIVE DEVICE FOR ELASTIC WAVES

### A. Wave speeds and refractive index

In this section, we design refractive devices that steer SV- and P-waves in different directions to split them from each other. The refractive devices are based upon a solid with aligned parallel gaps as shown in Fig. 8, in which the

Xiaoshi Su and Andrew N. Norris

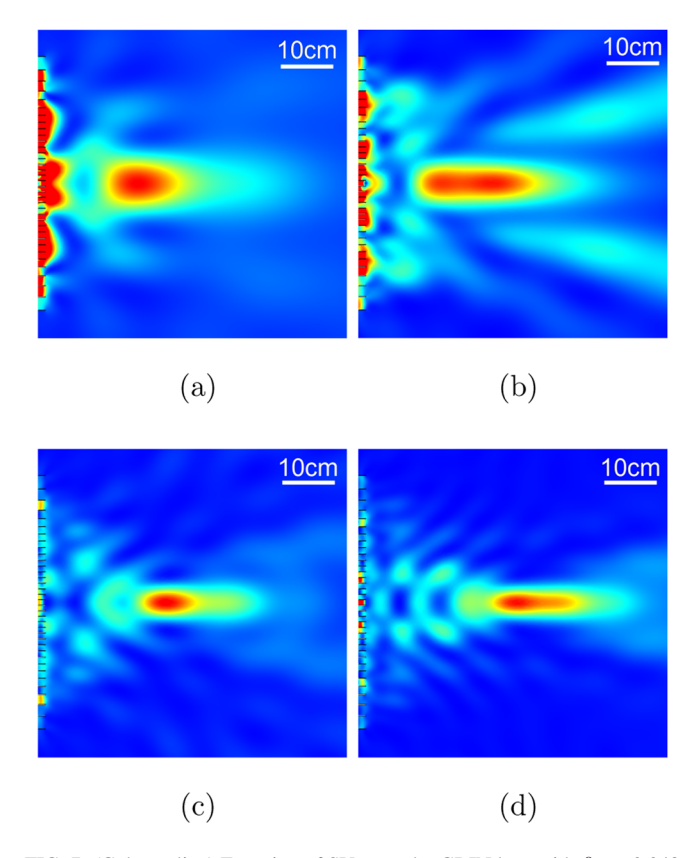


FIG. 7. (Color online) Focusing of SV-wave by GRIN lens with  $\beta = -0.048$  at (a) 20 kHz, (b) 30 kHz, (c) 40 kHz, and (d) 50 kHz.

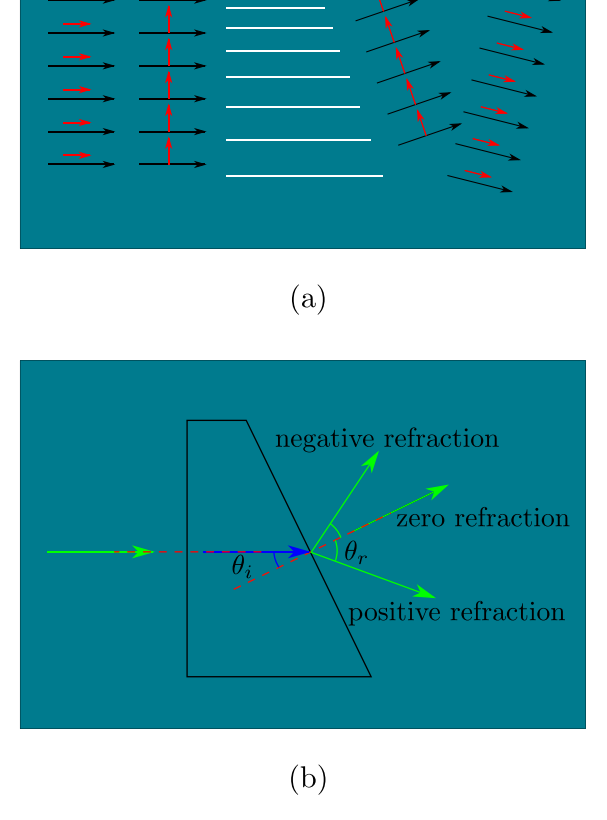


FIG. 8. (Color online) Refraction of elastic waves.

thin white strips are thin gaps with left end aligned vertically and the right end aligned with a slope. The effective plates have different lengths and thicknesses. Figure 8(a) illustrates the idea of steering SV- and P-waves in different directions. The long arrows indicate the propagation directions, the short arrows indicate the direction of particle motion, i.e., they are perpendicular to the propagation direction of SV-waves and parallel to the propagation direction of P-waves. Zero-refraction of SV-wave and positive refraction of P-wave are achieved based on the different wave speeds of the two wave and by selecting plate members that have high transmission for both SV- and P-waves.

The ratio of the length of the plate to the flexural wavelength is

$$\frac{L}{\lambda_F} = \frac{1}{2\pi} \left( \frac{E}{12\rho(1-\nu^2)\omega^2} \right)^{-1/4} \frac{L}{\sqrt{h}}.$$
 (17)

Equation (17) and  $t_F = L/c_F$  imply that the flexural waves travel through plates of the same  $L/\sqrt{h}$  in the same amount of time, and reach the other end with the same phase. Note that total transmission for an incident SV-wave occurs at  $\omega = \omega_n$ . Using  $t_F = L/c_F$  and Eq. (17), we have  $t_F = n\pi/\omega_n$  and  $L/\lambda_F = n/2$ , where n = 1, 2, 3, ... With these properties, we can select desired plate members for the solid structure, as shown in Fig. 8(a), and achieve zero-refractive index for SV-waves, i.e.,  $n_{SV} = 0$ . As shown in Fig. 9(a), this

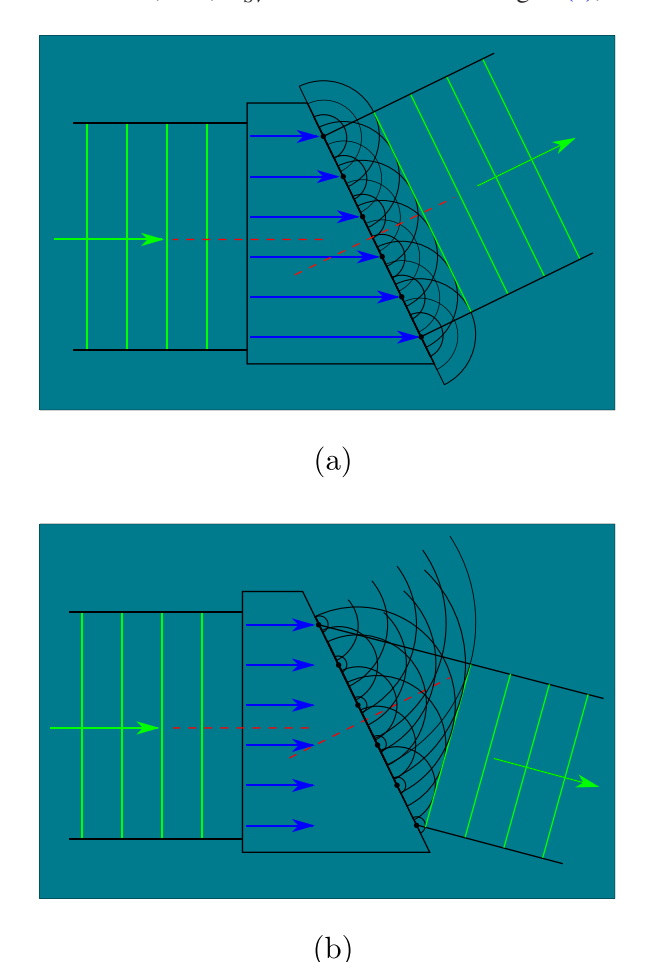


FIG. 9. (Color online) Diffraction of (a) SV- and (b) P-waves.

zero-refractive effect is independent of frequency since diffraction occurs simultaneously at the right ends of all the plates and forms a new wavefront which is parallel to the inclined edge of plate array, therefore the new SV-wave will propagate in the direction perpendicular to the edge. Notably, a normally incident SV-wave from the left side transmits to the right side keeping its original type, the transmitted P-wave is weak because the coupling mainly comes from the mode in the waveguide/plate. However, in the case of P-wave incidence, the physics of the longitudinal waves on the plate is different since the phase speed does not depend on the thickness of the plate. We consider the plate array as an effective medium in which the longitudinal wave speed in the lateral direction is constant, so that we have the refractive index  $n_P = c_P/c_L = (1 - \nu)/\sqrt{1 - 2\nu}$ , which only depends on the Poisson's ratio of the material. The refraction of P-wave can also be understood in terms of Huygens' principle as shown in Fig. 9(b). In summary, the refractive index for SV- and P-waves are

$$n_{SV} = \frac{\sin \theta_r}{\sin \theta_i} = 0, \tag{18}$$

$$n_P = \frac{\sin \theta_r}{\sin \theta_i} = \frac{1 - \nu}{\sqrt{1 - 2\nu}},\tag{19}$$

respectively.

The refractive device for SV- and P-waves is designed by choosing the thickness  $h_1$  and length  $L_1$  for the plate on the top, the thickness and length of the next plate can be calculated using the relations

$$h_i = \zeta L_i^2, \ L_{i+1} = L_i - \frac{a + h_i}{s},$$
 (20)

where the fixed value  $\zeta$  is chosen for a particular slope,  $L_i$  is the length of the plate, and  $L_{i+1}$  is the length of the next plate based on the chosen slope s.

We can also design negative-index metamaterial, i.e.,  $n_{SV} < 0$ , by varying the flexural wave travel time in the plates. If the thickness of the plates are the same and we use a similar structure as Fig. 8(a), then the refractive index is  $n_{SV} = [2E(1-\nu)/\rho(1+\nu)h^2\omega^2]^{1/4}$ , which varies with frequency.

# B. Example of refractive device

Using aluminum as the material, we choose the first plate with the dimensions  $h_1 = 0.005$  m,  $L_1 = 0.1$  m, and gap width a = 0.001 m. We also choose the parameters s = -3 and  $\zeta = 0.5$ , then the length and thickness of other plates are calculated using Eq. (20). In this example, we take the same modification term  $\beta$  for each plate for convenience, the optimal results are obtained when  $\beta = 0.15$ . Figure 10 shows SV-waves steered into the direction along the normal of the edge of plate array, i.e.,  $n_{SV} = 0$ . Figure 11 shows positive refraction of P-waves. In the case of P-wave incidence,  $\beta$  does not play a role but we keep using the same value for better comparison. The simulation results clearly show that the angles of transmitted waves are independent of

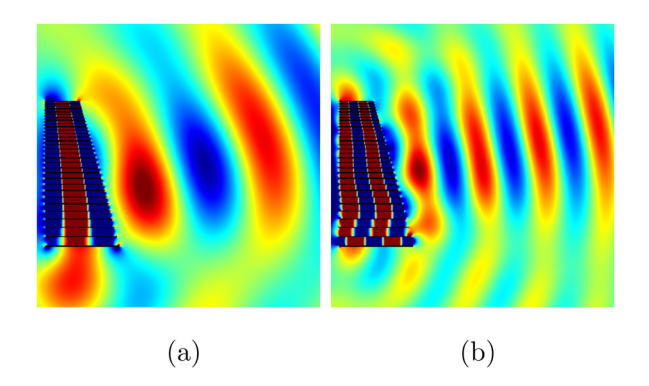


FIG. 10. (Color online) Zero SV-wave refraction at (a) 10 kHz and (b) 20 kHz.

frequency, because the plate array is designed so that the refractive index for both flexural wave and longitudinal wave are independent of frequency.

# V. ASYMMETRIC TRANSMISSION DEVICE FOR ELASTIC WAVES

# A. Mode conversion of P-wave and critical angle

The asymmetric transmission effect of P-waves is investigated in a solid with a flat free surface. As shown in Fig. 12(a) the energy carried by the incident P-wave from the left side at a specific angle  $\theta_P$  cannot transmit through the parallel gaps, and therefore will not be detected beyond them. However, if the P-wave is incident from the right side of the white slits at the angle  $\theta'_{P}$  as shown in Fig. 12(b), the energy will transmit to the left side efficiently. This transmission asymmetry can be achieved when the P-wave is incident from the left side at a critical incident angle, at which total conversion to SV-waves occurs. An array of parallel gaps perpendicular to the propagation direction of the reflected SV-wave can stop the SV-wave but will let P-waves incident from the right side travel through. In this section, we show the equations for mode conversion, and find the critical angle for total conversion from P- to SV-wave, which will be used in the design of the asymmetric transmission device in Sec. VB.

Assuming an incident P-wave at angle  $\theta_0$  with respect to the surface normal and amplitude  $A_0$ , the amplitudes of the

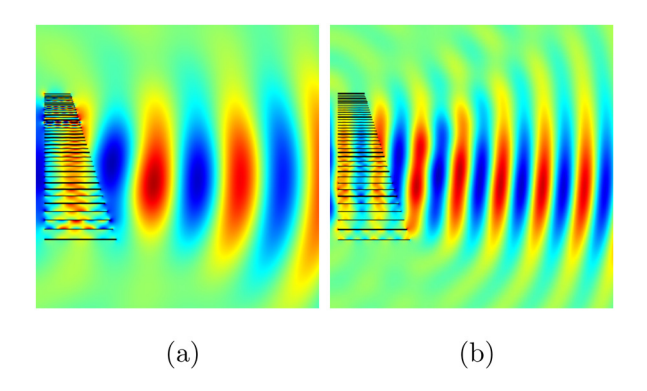


FIG. 11. (Color online) Positive P-wave refraction at (a) 20 kHz and (b) 40 kHz.

Xiaoshi Su and Andrew N. Norris

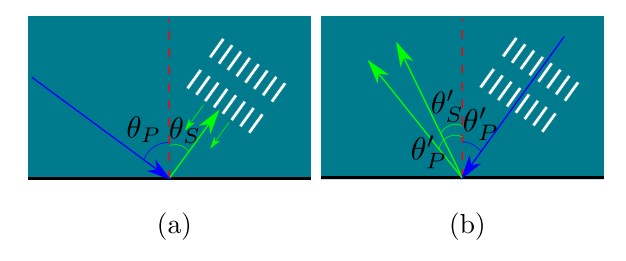


FIG. 12. (Color online) Asymmetric transmission. The horizontal black line represents the free boundary of a half-space, the rectangular white slits represent gaps, lines with arrow indicate the propagation direction.

reflected P- and SV-waves,  $A_1$  and  $A_2$ , are given by Eqs. (5.52) and (5.53) in Ref. 26 as

$$\frac{A_1}{A_0} = \frac{\sin 2\theta_0 \sin 2\theta_2 - \kappa^2 \cos^2 2\theta_2}{\sin 2\theta_0 \sin 2\theta_2 + \kappa^2 \cos^2 2\theta_2},\tag{21}$$

$$\frac{A_2}{A_0} = \frac{2\kappa \sin 2\theta_0 \cos 2\theta_2}{\sin 2\theta_0 \sin 2\theta_2 + \kappa^2 \cos^2 2\theta_2},\tag{22}$$

where  $\kappa = c_P/c_T = \sqrt{2(1-\nu)/(1-2\nu)}$  from Eq. (3), and  $\theta_2$  is the SV-reflection angle:  $\sin \theta_2 = \kappa^{-1} \sin \theta_0$ . Figure 13 shows the P-wave reflection coefficient. Setting  $A_1/A_0 = 0$  defines the critical incident angle  $\theta_0 = \theta_P$  for total conversion from P-wave to SV-wave.

For example, in a half-space made of material with the properties of brick ( $E=24\,\mathrm{GPa}$ ,  $\nu=0.12$ , and  $\rho=2300\,\mathrm{kg/m^3}$ ), the critical angle for total P-to-SV conversion is  $\theta_P=43.5^\circ$ , with SV reflection angle  $\theta_S=26.9^\circ$ . The energy plot from full FEM simulation is shown in Fig. 14(b) and matches well with the theoretical prediction.

# B. Example of asymmetric transmission device for P-wave

Figure 14 shows that brick-like material is very promising for the application of asymmetric elastic transmission. The critical angle for total conversion is large, providing enough space to place an array of rectangular gaps as shown in Fig. 12. Using brick as the material, we design an array of plates/gaps to stop SV-waves but let P-waves transmit

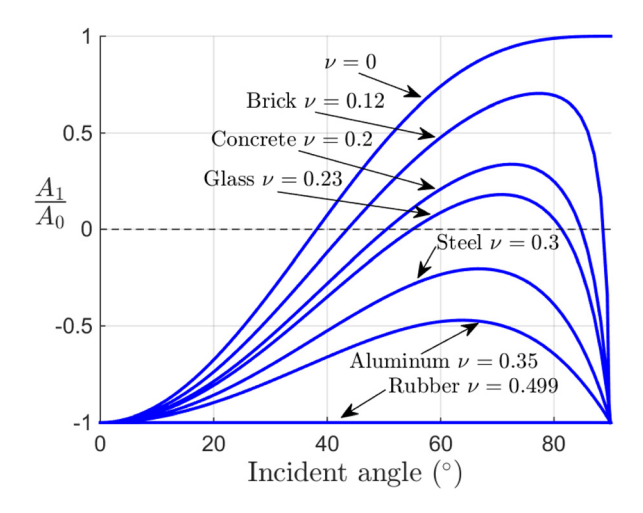


FIG. 13. (Color online) Amplitude ratio between incident and reflected P-wave of different materials, from Eq. (21).

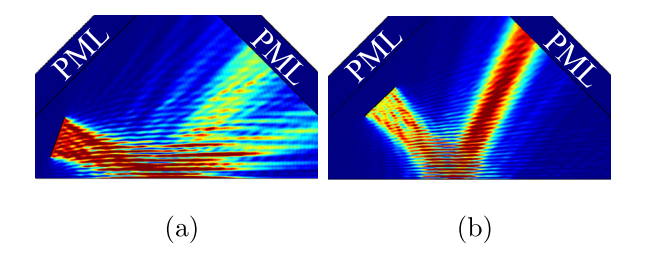


FIG. 14. (Color online) Mode conversion of P-wave at free boundary (bottom of the simulation domain) in brick without slits/gaps. (a) P-wave incidence from left side at non-critical angle  $\theta_0 = 70^{\circ}$ . (b) P-wave incidence from left side at critical angle  $\theta_0 = \theta_P \, (=43.5^{\circ})$ .

through. The dimensions of each gap is 0.001 m wide and 0.5 m long, and the thickness of the plate between gaps is 0.005 m. The gaps are aligned so that the angle between the normal of the gap array and the normal of the free boundary is  $\theta_S = 26.9^{\circ}$ . The horizontal line at the bottom of the simulation domain is the free boundary of the half-space. Figure 15(a) shows high energy reflection ( $|T|^2 < 9\%$ ) for P-wave incidence from the left side, Fig. 15(b) shows high energy transmission ( $|T|^2 > 94\%$ ) for P-waves incident from the right side.

#### VI. CONCLUSION

We have considered a novel configuration in solids made by parallel gaps that produce arrays of aligned "effective plates." The effects reported here arise from the coupling between SV-waves in the exterior elastic solid and flexural waves in the effective plates, and the coupling between P-waves in the bulk and longitudinal waves in the plates. The transmission and reflection coefficients for normally incident SV- and P-waves are calculated using thin plate theory. The overall agreement of the transmission spectrum of SV- and P-waves calculated using the analytical result and the full FEM simulation provides the basis for designing GRIN structures. The GRIN lens is designed by varying the thickness of the plates and demonstrated by full FEM simulation showing focusing effects over a wide range of frequency. The refractive device for SV- and P-waves is designed by fixing the ratio between L and  $\sqrt{h}$  and choosing the slope of the edge of the plate array. It is also calculated that the refractive index for flexural waves is 0 and is

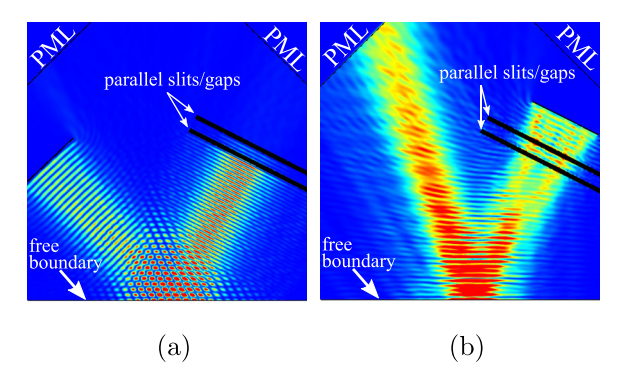


FIG. 15. (Color online) Asymmetric transmission effect at f = 21.6 kHz. (a) P-wave incident from the left side with  $\theta_0 = \theta_P$  (=43.5°). (b) SV-wave incident from the right side with  $\theta_0 = \theta_S$  (=26.9°).

independent of frequency and material properties, while the refractive index for longitudinal waves depends on the Poisson's ratio of the material. The one-way effect for P-waves is sensitive to frequency and is, therefore, a multiband effect. In summary, our analytical model of elastic waves through aligned parallel gaps provides a new approach to focus, steer, split, and stop elastic waves.

#### **ACKNOWLEDGMENTS**

The authors thank Dr. Alfonso Climente for advice and comments. This work was supported by ONR through MURI Grant No. N00014-13-1-0631.

- <sup>1</sup>A.-C. Hladky-Hennion, J. O. Vasseur, G. Haw, C. Croënne, L. Haumesser, and A. N. Norris, "Negative refraction of acoustic waves using a foam-like metallic structure," Appl. Phys. Lett. 102(14), 144103 (2013).
- <sup>2</sup>A. Climente, D. Torrent, and J. Sanchez-Dehesa, "Sound focusing by gradient index sonic lenses," Appl. Phys. Lett. **97**(10), 104103 (2010).
- <sup>3</sup>R. Fleury, D. L. Sounas, C. F. Sieck, M. R. Haberman, and A. Alu, "Sound isolation and giant linear nonreciprocity in a compact acoustic circulator," Science **343**(6170), 516–519 (2014).
- <sup>4</sup>B.-I. Popa and S. A. Cummer, "Non-reciprocal and highly nonlinear active acoustic metamaterials," Nat. Commun. **5**, 3398 (2014).
- <sup>5</sup>Z. Liu, Z. Zhang, Y. Mao, Y. Y. Zhu, Z. Yang, C. T. Chan, and P. Sheng, "Locally resonant sonic materials," Science **289**(5485), 1734–1736 (2000).
- <sup>6</sup>X. Zhang and Z. Liu, "Negative refraction of acoustic waves in twodimensional phononic crystals," Appl. Phys. Lett. 85(2), 341–343 (2004).
- <sup>7</sup>Z. Liang and J. Li, "Extreme acoustic metamaterial by coiling up space," Phys. Rev. Lett. **108**(11), 114301 (2012).
- <sup>8</sup>B. Liang, B. Yuan, and J.-C. Cheng, "Acoustic diode: Rectification of acoustic energy flux in one-dimensional systems," Phys. Rev. Lett. **103**(10), 104301 (2009).
- <sup>9</sup>B. Liang, X. S. Guo, J. Tu, D. Zhang, and J. C. Cheng, "An acoustic rectifier," Nat. Mater. **9**(12), 989–992 (2010).
- <sup>10</sup>W. Kan, B. Liang, X. Zhu, X. Zou, J. Yang, and J. Cheng, "Acoustic one-way frequency up-converter with high transmission efficiency," J. Appl. Phys. 114(13), 134508 (2013).
- <sup>11</sup>X.-F. Li, X. Ni, L. Feng, M.-H. Lu, C. He, and Y.-F. Chen, "Tunable uni-directional sound propagation through a sonic-crystal-based acoustic diode," Phys. Rev. Lett. **106**(8), 084301 (2011).

- <sup>12</sup>Y. Li, J. Tu, B. Liang, X. S. Guo, D. Zhang, and J. C. Cheng, "Unidirectional acoustic transmission based on source pattern reconstruction," J. Appl. Phys. 112(6), 064504 (2012).
- <sup>13</sup>Y. Li, B. Liang, Z.-M. Gu, X.-Y. Zou, and J.-C. Cheng, "Unidirectional acoustic transmission through a prism with near-zero refractive index," Appl. Phys. Lett. 103(5), 053505 (2013).
- <sup>14</sup>Y.-F. Zhu, X.-Y. Zou, B. Liang, and J.-C. Cheng, "Broadband unidirectional transmission of sound in unblocked channel," Appl. Phys. Lett. 106(17), 173508 (2015).
- <sup>15</sup>A. Climente, D. Torrent, and J. Sanchez-Dehesa, "Gradient index lenses for flexural waves based on thickness variations," Appl. Phys. Lett. 105(6), 064101 (2014).
- <sup>16</sup>B. Morvan, A. Tinel, A.-C. Hladky-Hennion, J. Vasseur, and B. Dubus, "Experimental demonstration of the negative refraction of a transverse elastic wave in a two-dimensional solid phononic crystal," Appl. Phys. Lett. 96(10), 101905 (2010).
- <sup>17</sup>J. Pierre, O. Boyko, L. Belliard, J. O. Vasseur, and B. Bonello, "Negative refraction of zero order flexural lamb waves through a two-dimensional phononic crystal," Appl. Phys. Lett. 97(12), 121919 (2010).
- <sup>18</sup>M. Farhat, S. Guenneau, S. Enoch, A. B. Movchan, and G. G. Petursson, "Focussing bending waves via negative refraction in perforated thin plates," Appl. Phys. Lett. 96(8), 081909 (2010).
- <sup>19</sup>M. Dubois, M. Farhat, E. Bossy, S. Enoch, S. Guenneau, and P. Sebbah, "Flat lens for pulse focusing of elastic waves in thin plates," Appl. Phys. Lett. 103(7), 071915 (2013).
- <sup>20</sup>R. Zhu, X. N. Liu, G. K. Hu, C. T. Sun, and G. L. Huang, "Negative refraction of elastic waves at the deep-subwavelength scale in a single-phase metamaterial," Nat. Commun. 5, 5510 (2014).
- <sup>21</sup>Z. Chang, H.-Y. Guo, B. Li, and X.-Q. Feng, "Disentangling longitudinal and shear elastic waves by neo-Hookean soft devices," Appl. Phys. Lett. 106(16), 161903 (2015).
- <sup>22</sup>X. Zhu, X. Zou, B. Liang, and J. Cheng, "One-way mode transmission in one-dimensional phononic crystal plates," J. Appl. Phys. **108**(12), 124909 (2010).
- <sup>23</sup>X. Zhou and G. Hu, "Analytic model of elastic metamaterials with local resonances," Phys. Rev. B **79**(19), 195109 (2009).
- <sup>24</sup>Y. Lai, Y. Wu, P. Sheng, and Z.-Q. Zhang, "Hybrid elastic solids," Nat. Mater. 10(8), 620–624 (2011).
- <sup>25</sup>A. Spadoni and C. Daraio, "Generation and control of sound bullets with a nonlinear acoustic lens," Proc. Natl. Acad. Sci. 107(16), 7230–7234 (2010).
- <sup>26</sup>J. D. Achenbach, Wave Propagation in Elastic Solids (North Holland, Amsterdam, 1987), p. 175.